P.309

EnKF Assimilation of Cloud Properties Retrieved From GOES

Thomas A. Jones[1,*] and David J. Stensrud[1,2]
1. Cooperative Institute for Mesoscale Meteorological Studies, University of Oklahoma
2. NOAA/OAR/National Severe Storms Laboratory, Norman, OK

Abstract

Assimilation of various forms of satellite data into numerical weather prediction models has led to a significant increase in global forecast skill during the past 25 years. Only recently have these efforts begun to be transitioned to convective-scale forecasts and initial research has shown promising results. One particular challenge in convective-scale data assimilation is properly identifying the location and intensity of cloud properties and the characteristics of the surrounding environment prior to initiating forecasts. To examine whether or not hi-resolution satellite data can provide value added information, this research assimilates cloud and humidity variables derived from Geostationary Operation Environmental Satellite (GOES) Imager cloud property retrievals.

The hypothesis posed by this research is that satellite derived cloud properties can provide information on the atmospheric state within and surrounding clouds that will enable an improved model analysis. Traditional atmospheric observations are assimilated into the WRF-ARW model using a 36 member Ensemble Kalman Filter (EnKF) assimilation technique over a continental U.S. domain at a 15 km resolution. Cloud and humidity variables are then assimilated using the same technique on a 3 km nested grid domain centered around a severe weather event on 10 May 2010.

**** Corresponding Author Address:***
Dr. Thomas A. Jones
Thomas.Jones@noaa.gov

Mesoscale data assimilation begins at 1200 UTC and continues until 2100 UTC 10 May with the cloud variables assimilated at 15 minute intervals within the nested grid from 1800 to 2100 UTC. The impacts of satellite data assimilation are assessed by comparing two identical model experiments: one with (CLD) and one without the satellite data assimilated (NOCLD).

WRF-DART assimilates ~90% of the available data with a combination of cloud-free and cloudy observations near the surface with primarily cloud-free data being assimilated aloft. Observation diagnostics indicate that assimilation of these data noticeably reduces 850 hPa bias and root mean square error (RMSE) for cloud liquid water content and, to a lesser extent, relative humidity after 2000 UTC. Comparing NOCLD and CLD analyses of QCLOUD at 2045 UTC for several pressure levels shows several locations where differences in the QCLOUD analyses exist. Interestingly at 900 and 850 hPa, the difference patterns in eastern Oklahoma seem to match the wave patterns present in the clouds observed by GOES visible imagery at this time. This is due to a 5-10 km spatial shift in the location of the clouds depicted in the CLD analysis compared to the NOCLD analysis. The changes to the 2100 UTC analysis fields generate differences in one hour forecasts of simulated reflectivity forecasts, but neither model appears skillful over the other at this time. These results represent a preliminary overview of ongoing research, which should provide a better understanding of the potential

for assimilating cloud properties using EnKF methods.

1. Introduction

The Warn-on-Forecast (WoF) project was developed with the goal of improving convective-scale forecasts to the degree where forecasters will have confidence to issue warnings based in part on numerical weather prediction (NWP) output (Stensrud et al. 2009). NWP-based warnings require that the forecast be of high quality, resolution, and reliability. One emphasis of the WoF project is to develop new assimilation techniques to take advantage of the vast new array of observations coming online during the next five years (Stensrud et al. 2009). Significant advances in high-resolution NWP models have been made during the past decade by studying the impacts of assimilating radar reflectivity and velocity data. These data provide high temporal and spatial resolution observations of convection and near-storm environments and have been shown to substantially improve model analyses and short-term severe weather forecasts (e.g. Dowell et al. 2010). While radar data has proven to be a valuable asset for severe weather forecasting, satellites represent another source of remote sensing data that can provide additional information on cloud properties and the surrounding environment.

The Imager on the GOES satellites observes one visible and four infrared channels at horizontal resolutions of 4 km or less at a temporal resolution of less than one hour over the continental United States (CONUS) (Menzel and Purdom 1994). The GOES satellite also includes a sounder that observes 19 visible and infrared channels providing some information on the vertical characteristics of atmospheric temperature and moisture (Schmit et al. 2002). Data from both sensors can also be used to ascertain the location and properties of clouds in the atmosphere (Minnis et al. 2008a, Schreiner et al. 2001). One advantage of using satellite data in this fashion is that certain clouds may form into thunderstorms are visible from satellite imagery before they can be observed on radar since small cloud droplets ($r < 100$ μm) are relatively insensitive to scattering in the microwave spectrum ($\lambda = 10$ cm). These cloud properties can be used to adjust model parameters to better match observations and conversely remove clouds and precipitation from the model analysis if clouds are not detected by the satellite data (e.g. Yucel et al. 2002, 2003; Benedetti and Janiskova 2008; Lauwaet et al. 2011).

Using cloud properties retrieved from GOES Imager data at 30 minute intervals on 10 May 2010, we assess the potential impact on short term severe weather forecasts over the Southern Plains. The goal is to show that satellite derived cloud information can add useful information to the model analysis potentially leading to improved forecasts. With the upcoming launch of GOES-R in 2015 and the Advanced Baseline Imager (ABI) these cloud products will become available at higher spatial and temporal resolutions comparable to that available from operational radar data (Schmit et al. 2005). Furthermore, the increased spectral resolution of the GOES-R ABI allows for more accurate cloud property retrievals and well as additional cloud products over what is currently available. Thus, the potential for using satellite data for high-resolution severe weather forecasts will only increase in the future.

2. Data and model characteristics

a. GOES Satellite Data

GOES satellite cloud properties are generated using a retrieval algorithm developed at the Langley Research Center (LaRC) that combines the Visible Infrared Solar-Infrared Split-Window Technique (VISST), the Solar-infrared Infrared Split-window Technique (SIST), and the Solar-infrared Infrared Near-infrared Technique (SINT) (Minnis et al. 2008b; 2011). The first method is used during the day when visible spectrum data are available, otherwise a combination of the latter two are used. Hereafter, the combined retrieval algorithm is simply referred to as VISST. This algorithm uses the visible (0.65 μm), solar infrared (3.9 μm) and infrared (10.8 12.0 or 13.3 μm) channels sampled by the current generation of the GOES Imager (Menzel and Purdom 1994; Schmit et al. 2001; Minnis et al. 2008) to determine the presence of clouds. The retrieval algorithm begins by performing a simple comparison of observed 10.8 μm brightness temperature with a clear sky background. If the observed temperature is colder, then that pixel is defined as cloudy. If it is warmer, additional tests are performed that include another IR test (12.0 or 13.3 μm) and difference test between the solar-infrared channel (3.9 μm) and infrared (10.8 μm) channels, and if visible data are available, a simple test to determine if visible reflectance is greater than the expected clear-sky values.

If all tests are passed, that pixel is defined as cloudy. For all pixels determined to be cloudy, the algorithm uses a 4-channel radiative transfer model to match the calibrated radiances to theoretical models of water and ice-crystal size distributions. Atmospheric parameters necessary to solve for skin temperature, cloud height, and radiance attenuation corrections are taken from NWP analysis fields. Clear-sky radiances, surface emissivities and surface classifications necessary for the retrievals are obtained from the Clouds and Earth's Radiant Energy System (CERES) instrument located on either the Terra or Aqua polar orbiting research satellites. A full description of this algorithm is provided by Minnis et al. (2008b) and Minnis et al. (2011).

Validation of GOES cloud top and base heights with surface-based cloud radar and lidar observations at the Atmospheric Radiation Measurement (ARM) site near Lamont, Oklahoma found that GOES cloud heights retrieved during daytime hours are generally accurate to within ±1.0 km with a slight low bias noted (Smith et al. 2008). Uncertainties are greatest for thin cirrus clouds in the upper troposphere and smallest for single layer low-level stratus. Base heights for deep convection are also sometimes too high since lower level information cannot be ascertained due to the very opaque nature of these clouds. Converting ±1 km to pressure coordinates, uncertainty becomes approximately ±50 hPa in the mid-troposphere.

We use cloud top and cloud base pressure (CTP, CBP) between 1800 and 2100 UTC retrieved at 30 minute intervals from the Imager on GOES-East (GOES-13) over the Southern Plains domain to generate a dataset of cloud and humidity variables that can be assimilated into NWP models. GOES data resolution is reduced to 3 km by sampling every third pixel prior to assimilation as higher resolution features would not be resolved by the 3 km resolution model grid used here. To better simulate the temporal resolution that will be available with GOES-R data, 30 minute satellite products are interpolated to generate data at 15 minute time intervals prior to deriving the cloud microphysical properties and humidity data for assimilation.

b. WRF-DART characteristics

The NWP model selected for this data impact study is the Advanced Weather Research and Forecasting (WRF-ARW) model version 3.2.1 using the Thompson microphysics scheme (Skamarock et al. 2008; Thompson et al. 2004). A 15-km domain covering most of the contiguous 48-states (CONUS) is defined with 51 vertical levels stretching from the surface up to 50 hPa. A parallel filter from the Data Assimilation Research Testbed (DART) software assimilates atmospheric observations including cloud properties, into WRF using an Ensemble Kalman Filter (EnKF) technique (Anderson et al. 2009). The primary advantage of this approach is that it provides a flow dependent and dynamically evolving estimate of the background error covariance for assimilated observations (Kalman 1960). Initial and boundary conditions are obtained from the 1200 UTC 10 May 2010 NAM model forecast fields. The data assimilation cycle starts at 1200 UTC 10 May 2010 and continues for 9 hours until 2100 UTC using traditional surface, marine, aircraft, and radiosonde observations. More detailed model characteristics used for the mesoscale assimilation can be found in Jones and Stensrud (2012). Using the mesoscale analyses as boundary conditions, a 3 km nested domain is generated over the area of the most intense observed convection with ensemble forecasts extending out to 0000 UTC 11 May. Two nests are created for comparison one with (CLD) and one without (NOCLD) satellite cloud data assimilated. For these data, the horizontal localization radius is 12 km and the vertical localization 4 km, similar to that currently used for radar data assimilation.

Since it is difficult to assimilate cloud properties such as CTP and cloud liquid (and ice) water paths (CWLP, CIWP) directly into NWP models, we generate 3-D arrays for atmospheric relative humidity (RH), cloud liquid water (QCLOUD), cloud ice (QICE), graupel (QGRAUP) and rainfall (QRAIN) using the same horizontal resolution as the satellite data and set the values according to the cloud observations. If no clouds are detected, then QCLOUD, QICE, QGRAUP, and QRAIN are set to zero for the atmospheric column at that location. RH remains defined as missing. Where GOES retrieves CTP and CBP information, RH is set to 100% between CTP and CBP to indicate to the model the presence of saturated air within the atmospheric column where a cloud is detected. CLWP is not assimilated in this research as the appropriate forward operator necessary to related total column CLWP to the vertical profile of CLW (and cloud ice) remains in development. Locations where satellite data are not available or otherwise do not pass the thresholds defined above remain set to missing. The "new" relative humidity and cloud microphysical variables are then assimilated into WRF-DART in the nested grid domain between 1800 and 2100 UTC at 15 minute intervals. The NOCLD ensemble is generated in the same manner, but with the new humidity and cloud variables set to evaluate-mode only.

3. Event Summary

Severe thunderstorms form in the afternoon and evening of 10 May 2010 associated with the passage of a shortwave trough across the Southern Plains, with dozens of damaging wind, severe hail, and tornado reports occurring between 2100 UTC 10 May and 0200 UTC 11 May (Fig. 1a). A surface low-pressure center deepens as it moves eastward through southern Kansas, trailing a dryline southward into central Oklahoma as shown at 2100 UTC (Fig. 1b). Ahead of the dryline, surface dewpoint exceeds 20 °C and south-southeasterly surface winds > 10 m s^{-1} blow over a large portion of central and southeastern Oklahoma. Surface temperatures range from ~34 °C in southwestern Oklahoma to below 20 °C in the northeastern part of the state where low clouds exist.

At higher levels, a strong wind field (> 40 ms^{-1} at 500 hPa) results in storm motions in excess of 25 ms^{-1} creating more than ample storm relative helicity for tornadic supercells (0-3 km SREH > 500 m^2 s^{-2}, Fig. 1c, d). Convective available potential energy (CAPE) also exceeds 2500 J kg^{-1} throughout much of central and southeastern Oklahoma (Fig. 1d). Supercell thunderstorms develop ahead of the eastward progressing dryline initially in southern Kansas around 1800 UTC and in central and southern Oklahoma by 2000 and 2200 UTC, respectively. A second line of supercells initiates nearer the dryline itself after 2300 UTC and also moves eastward before moving into southeastern Oklahoma by 0100 UTC 11 May.

Visible satellite imagery from GOES-13 at 2045 UTC (no 2100 UTC image is available) shows a large area of low-level stratus clouds in eastern Oklahoma and the adjacent regions of Kansas and North Texas (Fig. 2). Within this cloud field, northwest to southeast oriented wave features are evident in addition to what appears to be some southwest to northeast cloud streaks above this layer in northeastern Oklahoma. Clear sky and dry air characterize the environment behind the dryline in western Oklahoma with a cumulus field corresponding to developing convection also present. WSR-88D radar reflectivity data from KTLX (Twin Lakes, Oklahoma) show that several convective cells have developed north of 36°N by this time with a corresponding cirrus shield stretching into Kansas interacting with ongoing convection there (not shown).

4. Data Assimilation

a. Data Location

Between 1800 and 2100 UTC, nearly 781,000 observations of QCLOUD, QICE, QGRAPUL, QNRAIN, and RH are assimilated into the nested domain (Table 1). For cloud microphysical and RH variables, approximately 90% and 60% of the total number of data points are successfully assimilated (Table 1). RH represents the smallest portion since they are only assimilated when the satellite detects a cloud at a particular set of levels, whereas instances of no cloud detection are much more frequent. Remaining data fail to satisfy outlier thresholds specified within DART. These data are assimilated within a 3-D volume from near the surface (950 hPa) up to approximately the tropopause at 200 hPa. Within this volume, both the areal coverage and the vertical extent of cloud and no-cloud features can be discerned. To illustrate this point, assimilated data at 2045 UTC are plotted at pressure levels of 900, 850, 700, and 500 hPa (Fig. 3). At 900 hPa, DART assimilates a large area of RH=100% data points over much of eastern Oklahoma, western Arkansas and southwestern Missouri with each point denoted as a diamond in Figure 3a. These data correspond well to the location low-level clouds evident on the GOES-13 visible imagery at this time (Fig. 2). Further westward, no-clouds are present at this layer resulting in the assimilation of zero values for each of the cloud microphysical variables such as QCLOUD (black dots). Assimilated sample size between QCLOUD and RH is comparable at 900 hPa (766 vs. 592) given the large areal coverage of both clear and cloudy regions. No data points are plotted when either the retrieval algorithm fails to generate valid data or DART rejects incoming data as outliers.

Increasing in height to 850 hPa, the general patterns remain the same, but with fewer saturated relative humidity points being assimilated offset by a larger number of null microphysical variables (Fig. 3b). The change in height of the cloud properties corresponds to changes in CBP and CTP values retrieved from GOES. Above the CTP, assimilated data switch from RH=100% and cloud microphysical variables set to missing to cloud microphysical values becoming zero and RH values now set to missing. Beginning at 700 hPa and extending upward to 500 hPa, almost no saturated RH data points are being assimilated in eastern Oklahoma as the tops of most of these clouds lie lower in the atmosphere (Fig. 3c, d). In west-central Oklahoma, deeper clouds are detected by the satellite associated with the developing cumulus field evident in Figure 2 and result in the assimilation of a few saturated RH data points at several locations (Fig. 3d). The changes in the spatial and vertical characteristics of cloud microphysical properties and environmental humidity roughly depicts the location of cloudy vs. non-cloudy regions which when assimilated into WRF should result in an adjusted and hopefully improved model analysis.

b. Diagnostics

To the authors' knowledge, direct assimilation of cloud microphysical variables derived from satellite observations has not been previously undertaken within a WRF-DART framework. Thus, it is important to verify that these variables are being successfully assimilated and interpreted correctly. At every 15 minute time interval between 1800 and 2100 UTC, bias, root mean square error (RMSE), and total spread (TSPRD) are computed between the observations and the analysis. Figure 4 shows a time series of these statistics for QCLOUD and RH between 1800 and 2100 UTC at 850 hPa. Bias and RMSE for QCLOUD generally decrease out to 2000 UTC to near 0.25 g kg^{-1} and 0.55 g kg^{-1} respectively before increasing slightly thereafter (Fig. 4a). Between 1800 and 2000 UTC, no saw-tooth pattern exists in QCLOUD bias or RMSE indicating that little change in the prior and posterior analysis fields (Fig. 4a). Only after 2000 UTC does the desired pattern become evident with drops noticeable in both at each time step following 2000 UTC. The magnitude of the drop also increases with time reaching 0.05 g kg^{-1} by the final iteration at 2100 UTC (Fig. 4a). Total spread remains roughly constant at 0.05 g kg^{-1} with the total number of assimilated observations ranging between 700 and 900 at each time step (Fig. 4c). Observation diagnostics for the other cloud microphysical variables are similar (not shown).

Where clouds are detected from the satellite data, the RH at those locations is set to 100% generating 200 to 300 assimilated observations at each time step (Fig. 4c). Bias remains near –8% for all assimilation times indicating the model is too dry compared to the observations (Fig. 4b). Corresponding RMSE is approximately 10%. Differences between prior and posterior RH diagnostics are small until the final assimilation cycles after 2030 UTC. Here, bias and RMSE in the posterior analysis decrease approximately 0.5% with the improvement also increasing as a function of time, though this is difficult to visualize in Figure 4. This is an indication that the assimilation of saturated humidity values near the locations of clouds reduces an inherent dry bias present in the NOCLD analysis to some degree. However, the magnitude of these differences is smaller and takes longer to become evident than desired. Ideally, the saw-tooth patterns would become apparent after a couple of assimilation iterations. Thus, it would appear the assimilation techniques used here are not taking full advantage of the satellite data.

c. Impact on WRF 2045 UTC analyses

To visualize the effects of assimilating these data, we examine the difference in ensemble mean QCLOUD between NOCLD and CLD runs at 2045 UTC at the same levels shown in Figure 3. At 900 hPa, differences in QCLOUD on the order of 10^{-2} g kg^{-1} are evident over much of the eastern half of Oklahoma and adjacent areas of Kansas (Fig. 5a). The largest differences occur in central Oklahoma ahead of the developing cumulus field located near dryline at –98.0°W (Fig. 2). Another area of noticeable differences occurs in southeastern Oklahoma near the boundary of total cloudy and partly cloudy conditions at 34.5°N, -96.0°W (Fig. 2). Most differences are confined to the regions where saturated data points are assimilated with differences where null cloud microphysics variables are assimilated being negligible. Neither CLD nor NOCLD generate any significant cloud liquid water west of the dryline, so assimilating null cloud microphysical values here would have little effect. At 850 hPa, the areal coverage of differences in QCLOUD is smaller than at 900 hPa, but shows some interesting features compared to the location of assimilated observations and visible imagery. The greatest differences occur in southwestern Missouri and southeastern Oklahoma (Fig. 5b). A close examination of the differences in southeast Oklahoma shows that they seem to be oriented in a northwest-to-southeast orientation, which is remarkably similar to the orientation of the wave features evident in the visible imagery at this time (Fig. 2). Furthermore, the southwest-to-northeast wave pattern observed in the visible imagery in northeast Oklahoma also exists in the QCLOUD difference field (Fig. 2, 5b). Further research is underway to establish whether or not this qualitative similarity is indeed a result of WRF correctly assimilating of these variables. Other differences are present along the dryline with no differences observed in central Oklahoma due to the lack of data being assimilated in this region (Fig. 3b). At 700 and 500 hPa, neither NOCLD nor CLD generate any QCLOUD at these levels, which is consistent with the low top nature of the cloud cover in eastern Oklahoma (Fig. 5c, d). Most differences are confined to the deep cumulus clouds developing along the dryline. However, the spatial scale of these differences is small making their physical interpretation (if one exists) difficult. Differences in the total column IWP are also evident in west-central Oklahoma indicating that assimilating these variables affects convective features well above the freezing layer.

To better visualize the differences in QCLOUD wave patterns between NOCLD and CLD ensembles, a south-north cross section of QCLOUD at 850 hPa at 2045 UTC along the 95.5°W meridian between 34° - 36°N is provided in Figure 6a. Both models generate the same overall features with several peaks (thick clouds) and valleys (thin or no clouds) in QCLOUD. Some interesting differences exist and are represented in a rightward shift in the peaks of QCLOUD in the CLD analysis between 34° - 35°N (Fig. 6a). This indicates that the location of the clouds in the CLD analysis at 2045 UTC is slightly to the north than in NOCLD. The overall shift occurs over a distance between 5 – 10 km representing 2 or 3 model pixels. At 35.3°N, the peak in QCLOUD generated by CLD is shifted slightly to the left indicating a slight southward shift in the cloud location. North of 35.5°N, CLD and NOCLD are generally in close agreement. Differences between CLD and NOCLD cloud ice fields near the location of the developing convection are shown by plotting total column IWP generated from CLD and NOCLD ensembles at 2045 UTC along the 98.7°W meridian between 35° - 37°N (Fig. 6b). Between 35.5° - 36.0°N and at 36.3°N, CLD generates less cloud ice compared to NOCLD indicating that the assimilation of null cloud microphysical values derived from the satellite data correctly reduces cloud cover in the model analysis where none exists in observations.

The evidence strongly suggests that the satellite-derived data are being successfully assimilated and are nudging the analysis closer towards observations. The largest differences occur in the regions of either low-level cloud cover below 800 hPa and where no clouds are detected over large regions. While the magnitudes of these differences in QCLOUD and RH are often small, they do occur over large areas at low levels.

5. Forecast evaluation

The effects of assimilating the GOES derived cloud and humidity variables on forecast convection are assessed by comparing the probability of simulated radar reflectivity from CLD and NOCLD ensembles with observed radar reflectivity from the KTLX WSR-88D radar at 2 km above ground level. Regions where the probability of simulated reflectivity above 25 dBZ exceeds 50% are shaded for one hour NCDLD and CLD forecasts at 2200 UTC (Fig. 7). WSR-88D reflectivity data indicates well-developed convection is ongoing in three concentrated areas in Oklahoma near 36.5°, 35.5°, and 34.2°N (Fig. 7a, b). The location of the dryline is also evident in the clear-air returns behind the ongoing convection. Both NO-CLOUD and CLD models produce simulated reflectivity generally corresponding to the southern two regions of ongoing convection, though the forecast is too far west compared to observations. The area covered by the 50% contour is somewhat larger in the CLD forecast (Fig. 7b). Neither model appears skillful over the other, though this result is not unexpected given the preliminary nature of this research. More important is that assimilation of these satellite-derived variables yields a measurable difference in the convective scale forecast.

6. Summary

This research represents an early attempt at assimilating cloud microphysical properties and atmospheric humidity derived from high resolution satellite data using an EnKF modeling approach. Preliminary results indicate that WRF-DART correctly assimilates these variables in a manner that is physically consistent with observations. However, it currently takes two hours before the impacts of assimilating these data produce an improvement in the model analysis fields. The greatest impacts occur near low-level cloud regions, which is most evident in eastern Oklahoma at 900 and 850 hPa. Assimilation of null cloud microphysical properties also appears to produce impacts in western Oklahoma corresponding to the location of the developing convection. Difference patterns in QCLOUD between NOCLD and CLD output are remarkably similar to the wave-like cloud patterns present in the GOES visible imagery. Analysis indicates that assimilation of these data yields a 5 – 10 km displacement in the QCLOUD (and IWP) analyses near the end of the assimilation cycle compared to NOCLD. Further work is required to verify the specific mechanisms leading to this finding. Differences in one hour simulated reflectivity forecasts also occur, but neither model appears to be skillful over the other.

Many challenges remain in order to prove EnKF assimilation of satellite derived humidity and cloud microphysical variables at these scales can increase forecast skill in models. That it takes two hours before significant impacts are noticeable in the observation diagnostics is a strong indication that the satellite data is not being used to its full potential. It is likely that varying cloud microphysical schemes within the model will have a significant impact how these properties are assimilated. Further research is required to determine which schemes are best suited to this task. Current vertical and horizontal localization radii are based off those used for similar resolution radar data assimilation, but may not be completely valid for satellite-derived products. Another major concern is the uncertainties and errors used for these variables during the assimilation process. In the case of a large number of null data points, normal assumptions about the distribution of model errors are likely not valid. Including satellite derived vertical profiles of CLWC and IWC only complicates this issue further. Despite these challenges, these preliminary results indicate that direct assimilation of these variables from satellite data can be useful in convective scale environments. Upcoming research is planned to address many of these challenges using idealized simulations of convection along with simulated satellite data to define the most robust methods possible for future real-data applications in the WoF project.

Acknowledgements

GOES Imager cloud property retrievals were kindly provided by Patrick Minnis at the Langley Research Center in Hampton, Virginia and processed specifically for this case by Rabindra Palikonda. Raw visible GOES imagery and WSR-88D level 2 radar reflectivity where retrieved from National Climate Data Center archives. This research was supported by the NOAA National Environmental Satellite, Data, and Information Service. Partial funding for this research was also provided by NOAA/Office of Oceanic and Atmospheric Research under NOAA–University of Oklahoma Cooperative Agreement NA17RJ1227, under the U.S. Department of Commerce.

References

Anderson, J. L., T. Hoar, K. Raeder, H. Liu, N. Collins, R. Torn, and A. Avellano, 2009: The Data Assimilation Research Testbed: A community data assimilation facility. *Bull. Amer. Meteor. Soc.*, **90**, 1283–1296.

Benedetti, A. and Janisková, M. 2008. Assimilation of MODIS Cloud Optical Depths in the 11 ECMWF *Model. Atmospheric Review*, **136**, 1727-1747.

Dowell, D. C., G. S. Romine and C. Snder, 2010: Ensemble storm-scale data assimilation and prediction for severe convective storms. Preprints, *25th Conference on Severe Local Storms*, Denver, CO, USA, Amer. Meteor. Soc., 9.5.

Jones, T.A. and D. J. Stensrud, 2012: Assimilating AIRS temperature and mixing ratio profiles using an Ensemble Kalman Filter approach for convective-scale forecasts. *Wea. and Forecasting*, In Press.

Kalman, R.E., 1960: A new approach to linear filtering and prediction problems. *Journal of Basic Engineering*, **82**, 35–45.

Lauwaet, D., K. De Ridder, and P. Pandey, 2011: Assimilating remotely sensed cloud optical thickness into a mesoscale model. *Atmos. Chem. Phys. Discuss.*, **11**, 13355-13380

Menzel, W. P., and J. F. Purdom, 1994: Introducing GOES-I: The first of a new generation of geostationary operational environmental satellites. *Bull. Amer. Meteor. Soc.*, **75**, 757–781.

Minnis, P., L. Nguyen, R. Palikonda, P. W. Heck, D. A. Spangenberg, et al., 2008a: Near-real time cloud retrievals from operational and research meteorological satellites. *Proc. SPIE Europe Remote Sens. 2008*, Cardiff, Wales, UK, 15-18 September, **7107-2**, 8 pp.

Minnis, P., Q. Z. Trepte, S. Sun-Mack, Y. Chen, D. R. Doelling, et al., 2008b: Cloud detection in non-polar regions for CERES using TRMM VIRS and Terra and Aqua MODIS data. *IEEE Trans. Geosci. Remote Sens.*, **46**, 3857-3884.

Minnis, P., S. Sun-Mack, D. F. Young, P. W. Heck, D. P. Garber, et al., 2011: CERES Edition-2 cloud property retrievals using TRMM VIRS and Terra and Aqua MODIS data, Part I: Algorithms. *IEEE Trans. Geosci. Remote Sens.*, **49**, *11*, 4374-4400.

Schmit, T. J., E. M. Prins, A. J. Schreiner, and J. J. Gurka, 2001: Introducing the GOES-M imager. *Natl. Wea. Dig.*, **25**, 28–37.

Schmit, T. J., W. F. Feltz, W. P. Menzel, J. Jung, A. P. Noel, J. N. Heil, J. P. Nelson, and G. S. Wade, 2002: Validation and use of

GOES sounder moisture information. *Wea. and Forecasting*, **17**, 139-154.

Schmit, T. J., M. M. Gunshor, W. P. Menzel, J. J. Gurka, J. Li, A. S. Bachmeier, 2005: INTRODUCING THE NEXT-GENERATION ADVANCED BASELINE IMAGER ON GOES-R. *Bull. Amer. Meteor. Soc.*, **86**, 1079–1096.

Schreiner, A. J., T. J. Schmit, and W. P. Menzel, 2001: Observations and trends of clouds based on GOES sounder data. *J. Geophys. Res.*, **106**, 20349 – 20363.

Skamarock, W. C., J. B. Klemp, J. Dudhia, D. O. Gill, D. M. Barker, M. G. Duda, X-Y. Huang, W. Wang, and J. G. Powers, 2008: A description of the Advanced Research WRF version 3. NCAR Tech Note NCAR/TN-475+STR, 113 pp. [Available from UCAR Communications, P. O. Box 3000, Boulder, CO 80307.]

Smith, W. L., P. Minnis, H. Finney, R. Palikonda, and M. M. Khaiyer, 2008: An evaluation of operational GOES-derived single-layer cloud top heights with ARSCL over the ARM Southern Great Plains site. *Geophys. Res. Lett.*, **35**, L13820, doi:10.1029/2008GL034275.

Stensrud, D. J., M. Xue, L. J. Wicker, K. E. Kelleher, M. P. Foster, J. T. Schaefer, R. S. Schneider, S. G. Benjamin, S. S. Weygandt, J. T. Ferree, and J. P. Tuell, 2009: Convective-scale warn-on-forecast system. A vision for 2020. *Bull. Amer. Meteor. Soc.*, **90**, 1487-1499.

Thompson, G., R. M. Rasmussen, and K. Manning, 2004: Explicit forecasts of winter precipitation using an improved bulk microphysics scheme. Part I: Description and sensitivity analysis. Mon. Wea. Rev., **132**, 519–542.

Torn, R. D., G. J. Hakim, and C. Snyder, 2006: Boundary conditions for limited area ensemble Kalman filters. *Mon. Wea. Rev.,* **134**, 2490-2502.

Yucel, I., W. J. Shuttleworth, R. T. Pinker, L. Lu, and S. Sorooshian, 2002: Impact of ingesting satellite-derived cloud cover into the Regional Atmospheric Modeling System. *Mon. Wea. Rev.,* **130**, 610–628.

Yucel, I., W. J. Shuttleworth, X. Gao, and S. Sorooshian, 2003: Short-term performance of MM5 with cloud-cover assimilation from satellite observations. *Mon. Wea. Rev.*, **131,** 1797–1810.

Tables and Figures:

VARIABLE	TOTAL N	ASSIMILATED N	% ASSIM
QCLOUD	205482	187042	91.0
QICE	205482	190796	92.8
QRAIN	205482	190380	92.6
QGRAUP	205482	196392	92.6
RH	37189	22357	60.1
TOTAL	859117	780967	90.9

Table 1. Number of data points generated and successfully assimilated into WRF-DART between 1800 – 2100 UTC 10 May 2010. Note the number of null cloud microphysical data points far exceeds that for saturated RH data.

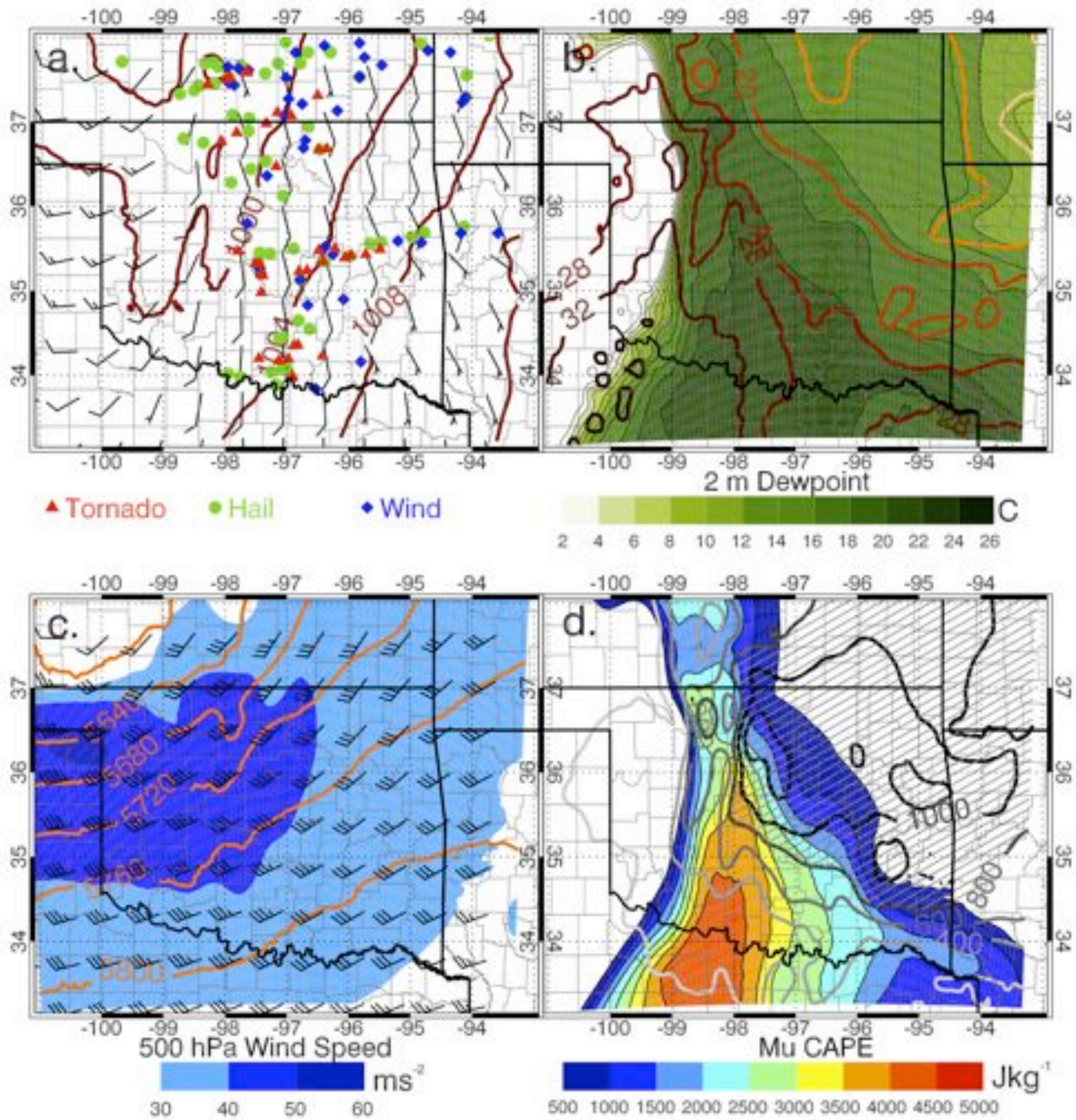

Figure 1. (a) Tornado, hail, and wind severe weather reports in the Southern Plains between 2100 UTC 10 May and 0200 UTC 11 May 2010 with surface winds speed and direction and mean sea level pressure (hPa) contours at 2100 UTC overlaid. Long barb = 10 ms^{-1} and short barb = 5 ms^{-1}. (b) Surface dewpoint and temperature (°C). (c) 500 hPa geopotential height field and wind velocity vectors (ms^{-1}). (d) CAPE (J kg^{-1}) and 0 – 3 km storm relatively helicity (SREH, m^{2}s^{-2}) all at 2100 UTC. Hatched areas indicate locations where SREH exceeds 800 m^{2}s^{-2}.

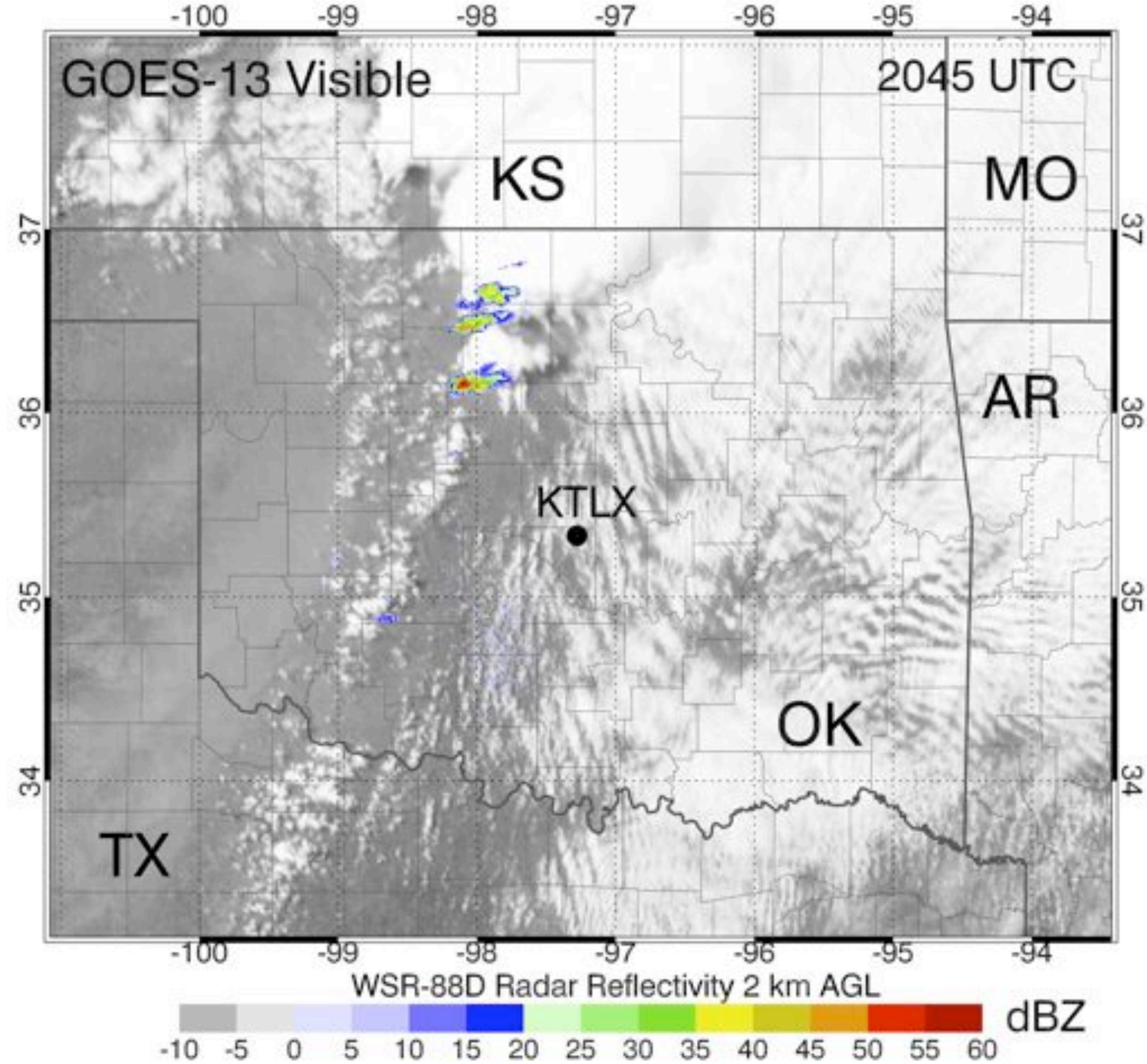

Figure 2. GOES-13 1 km resolution visible satellite imagery at 2045 UTC with WSR-88D radar reflectivity from KTLX overlaid.

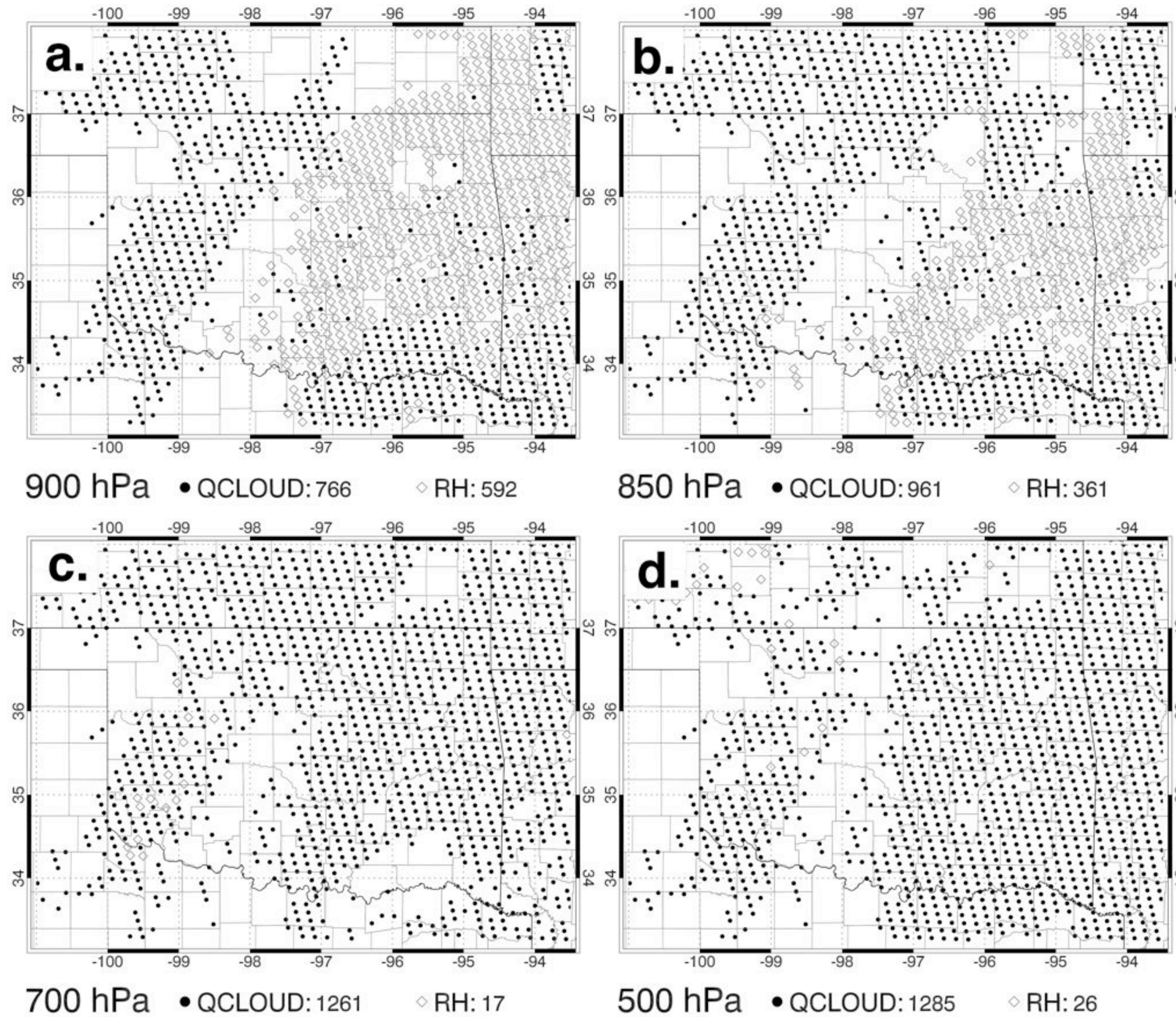

Figure 3. Assimilated QCLOUD (dots) and RH (diamonds) variables at 2045 UTC at 900 (a), 850 (b), 700 (c), and 500 hPa (d). White areas indicate regions where no valid GOES retrievals exist or are rejected by DART.

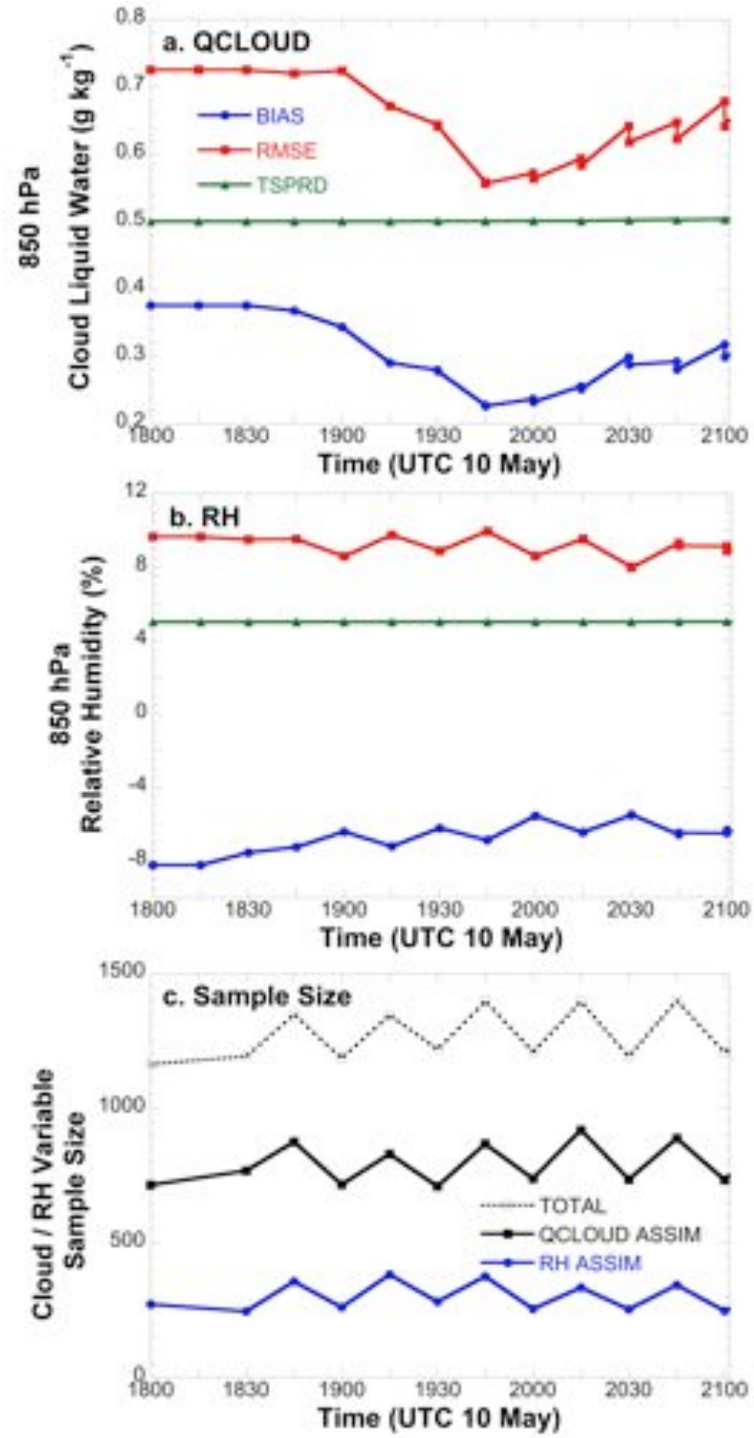

Figure 4. Observation diagnostics at 850 hPa for (a) QCLOUD and (b) RH showing model bias (blue), RMSE (red), and TSPRD (green) between model analyses and assimilated data before and after assimilation for each 15 minute cycle staring at 1800 UTC and continuing until 2100 UTC. Differences in bias and RMSE remain small until after 2000 UTC for QCLOUD and are not evident in RH on this scale. The latter only change by 0.5% at the final iteration. Total and assimilated sample size for each time step for QCLOUD and RH is provided in panel c.

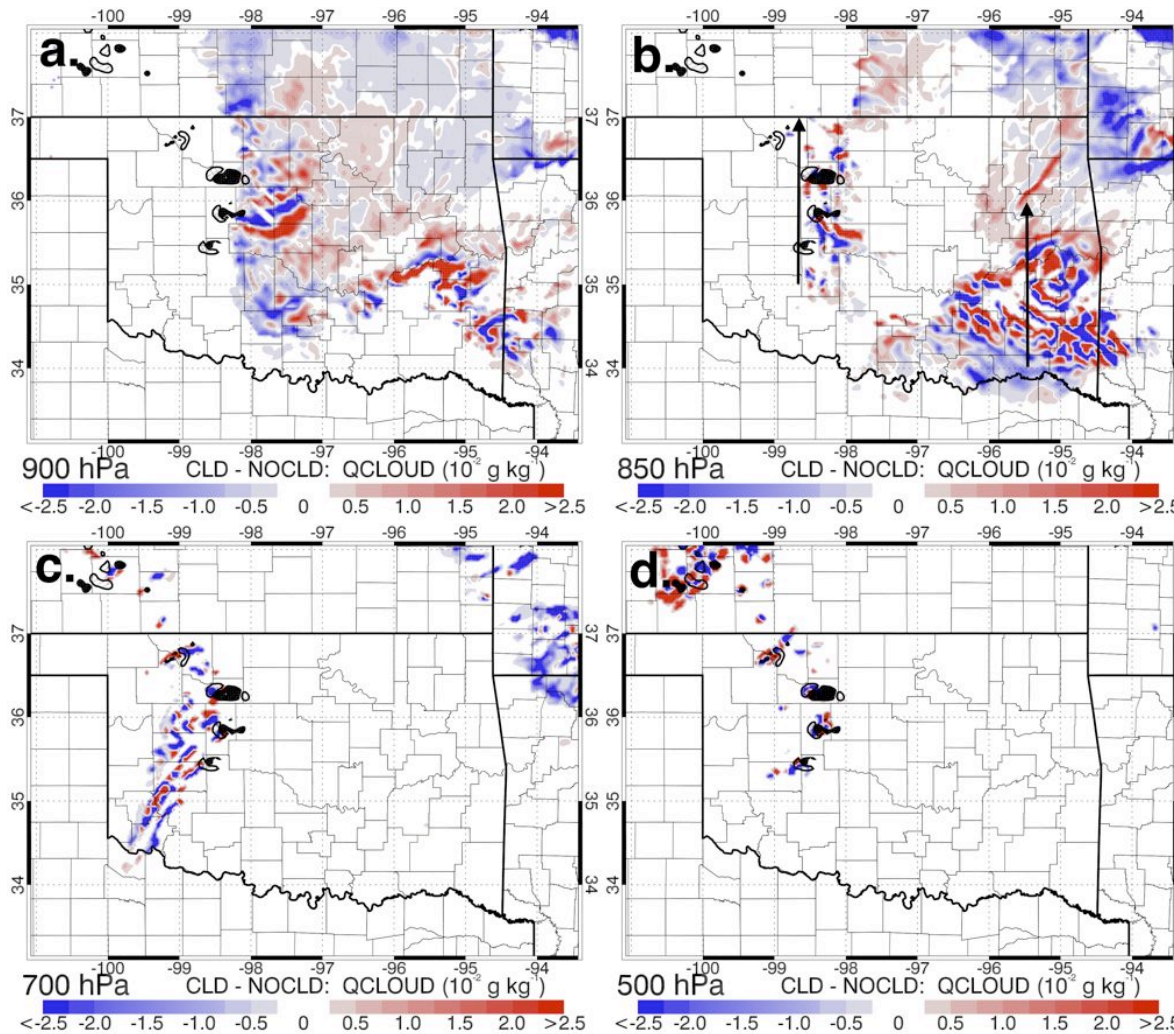

Figure 5. NOCLD minus CLD analyzed QCLOUD at (a) 900, (b) 850, (c) 700, and (d) 500 hPa at 2045 UTC. Red denotes where QCLOUD is greater in the CLD analysis while blue denotes where QCLOUD is less. Also plotted on each panel is where the difference in total column IWP derived from QICE is either positive or negative. Solid black denotes where IWP from CLD is greater and hatched areas where it is less. The locations of the cross sections in the following figure are overlaid on panel 5b.

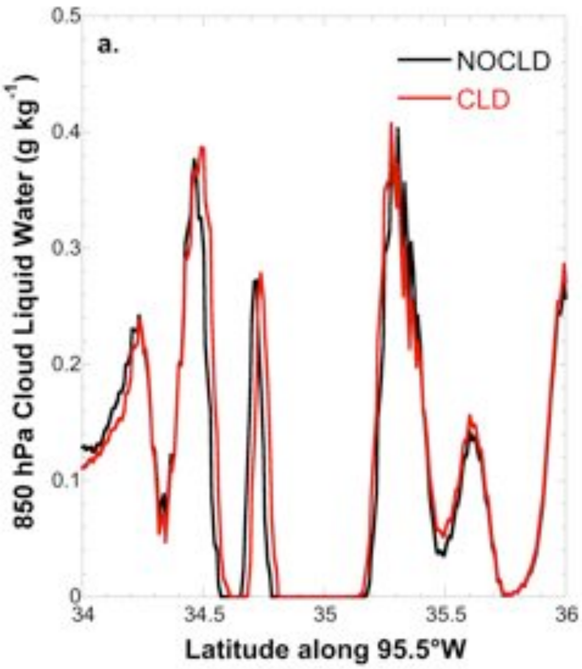

Figure 6. South-north cross sections of 850 hPa (a) QCLOUD and (b) IWP from NOCLD (black) and CLD (red) ensembles. Relative locations of each cross section are given in Figure 5b.

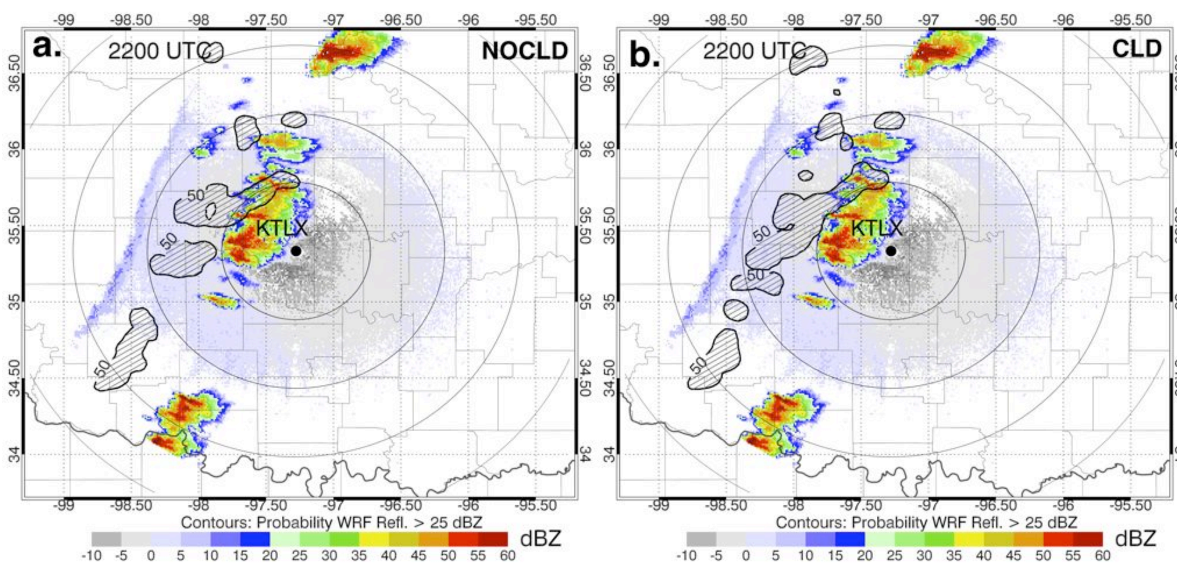

Figure 7. WSR-88D radar reflectivity at 2 km AGL from KTLX at 2200 UTC with the 50% probability of simulated radar reflectivity > 25 dBZ contour hatched in for (a) NOCLD and (b) CLD one hour forecasts.